JOURNAL OF AIRCRAFT
Vol. 44, No. 6, November–December 2007

Distributed Rate-Dependent Elastoslide Model for Elastomeric Lag Dampers

Wei Hu* and Norman M. Wereley†
University of Maryland, College Park, Maryland 20742

DOI: 10.2514/1.26409

To describe the nonlinear behavior of elastomeric dampers, a distributed rate-dependent elastoslide model is developed based on physically motivated damping mechanisms of a filled elastomer. Mathematically, the forced response of an elastomeric damper under a harmonic displacement excitation is developed from a summation of an integral of distributed yield force and a linear-spring force. This physically motivated model consists of rate-dependent elastoslide elements, using a distribution law to account for the yield force, and a parallel polymer residual stiffness. The selection of a yield-distribution function is based on an initial loading curve determined from force vs displacement hysteresis cycles over a broad amplitude range. The fidelity of this five-parameter time-domain model is justified by comparing measured and reconstructed damper responses, that is, steady-state hysteresis cycles, as well as by comparing complex modulus. The elastoslide model is formulated in the state space to improve ease of implementation into helicopter dynamics analyses.

I. Introduction

AN ELASTOMERIC damper has proven to be efficient for damping augmentation in helicopter rotors due to its simple design, low weight, and high reliability. However, filled elastomeric dampers exhibit significant nonlinearities [1]. Characteristics of the behavior of filled elastomers include 1) nonelliptical shear strain and stress hysteresis under sinusoidal excitation, 2) stiffness and damping dependence on amplitude, frequency, temperature, and even preloading conditions, 3) the Mullins effect, with reduction of stiffness at small strains, following cyclic deformation at large strains, and 4) low rates of stress relaxation and creep. Specifically, the large reduction of damping with increasing amplitude of harmonic displacement excitation leads to excessive size and weight of the dampers to accommodate all operating conditions. It was also found that highly damped elastomeric dampers demonstrated low loss factors at low amplitudes, resulting in unacceptable limit-cycle oscillations [2]. Therefore, a precise analytical model is necessary to describe the nonlinear behavior of an elastomeric damper and to determine its dynamic characteristics when implemented in a helicopter.

Complex moduli are effective in characterizing viscoelastic materials under harmonic excitation. Early modeling efforts focused on linearization using such complex moduli at a given harmonic, for which the storage modulus is a measure of the energy stored, and the loss modulus is a measure of the energy dissipated, over one period of oscillation. This model can be represented as a spring and a dashpot in parallel (that is, a Kelvin chain). The complex modulus is a linearization method in the frequency domain that replaces the nonlinear hysteresis loop with an equivalent ellipse and is only applicable to steady harmonic forced-response analysis. For nonlinear elastomeric materials, the complex moduli are also amplitude-dependent. Some researchers extended the basic Kelvin chain to a more complicated mechanism-based modeling approach to describe the nonlinear behavior of elastomers. Felker et al. [3] developed a nonlinear complex modulus model based on a single Kelvin chain, in which the spring force was a nonlinear function of the displacement and the damping force was a nonlinear function of displacement and velocity. This model was used to describe the amplitude-dependent moduli and to study dual-frequency damper motions. To display basic behavioral characteristics such as creep and relaxation, a viscoelastic solid can be represented as a spring in series with Kelvin elements (if a 1-K element is used, it is called a Zener model [4]). Gandhi and Chopra [5] developed a nonlinear viscoelastic solid model in which a nonlinear leading spring was used in series with a single linear Kelvin chain. Using this model, the variation of the analytical complex moduli with different amplitudes closely matched experimental data. The parameters in all of these models were identified using amplitude-dependent complex modulus data, and the nonlinear force vs displacement hysteresis behavior of elastomers cannot be captured using these models.

Kunz [6] used a nonlinear Kelvin chain to capture the nonlinear hysteresis behavior of an elastomeric damper. In this model, the stiffness was expressed as a fourth-order polynomial function of displacement, and the damping was described by a second-order polynomial function of velocity. Though it can predict the harmonic damper force rather well, this approach is only applicable to a particular amplitude and frequency. In the model developed by Tarzanin and Panda [7], the total damper force was represented by a nonlinear spring force and a nonlinear Coulomb friction-damping force. This model was based on single-frequency or harmonic data and was used to match energy dissipation per cycle. However, a step jump in predicted damper force was shown when velocity changed sign, which was unrealistic. Panda et al. [2] replaced the Coulomb friction-damping element with a variable friction-damping element for which the force was calculated based on the peak displacement of excitation when the velocity was zero. This model correlated well with experimental hysteresis data, but the effectiveness of this model over a range of amplitudes and frequencies has not been demonstrated in the literature. In a recent study, Krishnan [8] developed a model that consisted of a linear Kelvin chain and a parallel cubic spring element. Snyder [9] improved this model by adding an elastoslide element. Both models were developed to capture nonlinear elastomeric damper hysteresis cycles, but the model parameters were still amplitude- and frequency-dependent.

Alternative elastomeric models were developed using internal variable or nonlinear integral equations. Strganac [10] used a stress shift function to formulate a nonlinear time-domain model for elastomers, but the nonlinear integral formulation in the model was difficult to implement in traditional aeromechanical analysis. Lesieutre and Bianchini [11] developed the anelastic displacement

Received 9 July 2006; revision received 22 June 2007; accepted for publication 10 July 2007. Copyright © 2007 by Norman M. Wereley. Published by the American Institute of Aeronautics and Astronautics, Inc., with permission. Copies of this paper may be made for personal or internal use, on condition that the copier pay the $10.00 per-copy fee to the Copyright Clearance Center, Inc., 222 Rosewood Drive, Danvers, MA 01923; include the code 0021-8669/07 $10.00 in correspondence with the CCC.

*Research Associate, Alfred Gessow Rotorcraft Center, Department of Aerospace Engineering; weihu@umd.edu. Member AIAA.

†Professor, Alfred Gessow Rotorcraft Center, Department of Aerospace Engineering; wereley@umd.edu. Associate Fellow AIAA.

field (ADF) method to describe the frequency-dependent behavior of linear materials. It was based on the notion of scalar internal variables or augmenting thermodynamic fields (ATF) [12] that described the interaction of the displacement field with irreversible processes occurring at the material level. In the ADF approach, the effects of the thermodynamic processes were focused on the displacement field, which consists of both elastic and anelastic parts. The anelastic part may be further subdivided to consider the effects of multiple relaxation processes. Although there is no explicit physical interpretation when multi-anelastic elements are involved, one single ADF model is mechanically analogous to the Zener model.

To capture the characteristic nonlinear hysteretic behavior of elastomeric materials, Govindswamy et al. [13] developed a nonlinear ADF model in which the linear ADF parameters were replaced with nonlinear terms. The model captured the variations of the complex modulus with amplitude and performed as well in matching the strain–stress hysteresis. Furthermore, other functional forms for the ADF parameters were introduced to improve hysteresis loop predictions. Brackbill et al. [14] improved the nonlinear ADF model by adding rate-independent nonlinearity, in which friction-damping and linear-spring elements in parallel with the baseline nonlinear ADF model were used to provide additional amplitude-dependent relaxation behavior. As many as 16 parameters were used to construct the model. Although the complex moduli were fitted well in certain amplitude and frequency ranges, the performance of the model in predicting nonlinear hysteresis behavior could still be improved. Moreover, the process to determine model parameters was complicated by the fact that some parameters were chosen by empirical observation. In a recent study, Ramrakhyani et al. [15] developed an ADF-based model containing nonlinear fractional derivatives and frictional elements. This model used eight parameters instead of 16 parameters to capture the amplitude-dependent and mild frequency-dependent modulus. However, the prediction of hysteresis loops did not noticeably improve, and the determination of model parameters remains complicated.

Generally, most existing modeling efforts were based on the viscoelastic assumption for elastomeric materials. However, an elastomeric damper usually demonstrates triboelastic behavior [1], such that those damper models using linear or nonlinear Kelvin chain combinations cannot adequately capture the elastomeric behavior. Either the model parameters were amplitude-dependent or the model poorly described the hysteretic behavior of the elastomeric damper. Although in some modeling efforts Coulomb or friction damping was used to describe the rate-independent damping behavior significantly demonstrated by the elastomer, a single or even a finite number of Coulomb elements are not sufficient to adequately model damper force in response to sinusoidal excitation over a range of amplitudes and frequencies. The disadvantage for these modeling efforts is that the excitation amplitude must be known a priori to use these models effectively.

Thus, an efficient and accurate model for elastomeric dampers needs to be developed based on the damping mechanisms within the damper material. Physically, the amplitude-dependent behavior demonstrated by the elastomer is mostly based on the interaction between the filler and rubber compound inside the filled elastomeric materials [16]. Before large deformation of a filled elastomeric damper, an intact filler structure displays a large stiffness and small loss factor for small amplitudes. As the amplitude increases, the filler structure breaks, resulting in a stiffness reduction. However, the breaking of filler structures, which is similar to frictional behavior, increases the loss factor. As the amplitude increases further and the frictional effect is fully released, both stiffness and loss factor drop to lower levels, which then are maintained relatively constant by the remaining polymer chains.

Motivated by the preceding physical mechanisms, a number of researchers attempted to combine springs and frictional slides to represent the filler and rubber compound in filled rubbers or elastomers. As early as 1933, Timoshenko [17] suggested that the general hysteretic system consists of a large number of ideal elastoplastic elements with different yield levels. Iwan [18,19] further developed a distributed-element model to study the steady-state dynamic response of a hysteretic system. Instead of specifying a distribution function numerically to agree with experimental data, a constant band-limited statistical function was used to define yield properties of the slide elements in this model. This model proved successful in predicting steady-state frequency response of a hysteretic system using a method of linearization. However, the excitation amplitude must be known a priori when this model is applied in the analysis, which is only applicable in steady-state response prediction. The theory of triboelasticity [20] also stated that the behavior of a filled elastomer can be represented by a large or infinite number of alternate springs and frictional slides in series, and each slide has a constant yield force and each spring has a constant stiffness. Coveney et al. [1] developed a three-parameter standard triboelastic solid (STS) model based on the theory of triboelasticity and further developed a four-parameter rate-dependent triboelastic (RT) model. These models gave a satisfactory representation of the material behavior. However, because the yield force was fixed along different slides, these models showed less flexibility in representing the amplitude-dependent behavior for different filled-level materials.

Inspired by these models using elastoslide elements, we develop a distributed rate-dependent elastoslide model to describe the amplitude-dependent behavior for filled elastomeric dampers. Because a filled elastomer exhibits frictional behavior, this physically motivated model consists of a large number of rate-dependent elastoslide elements with different yield levels and a parallel linear-spring element. The elastoslide element is used to simulate the friction behavior demonstrated by the filler structure in the elastomer, and the linear spring represents the remaining polymer stiffness. Mathematically, the forced response of the elastomeric damper under a displacement excitation is developed from a summation of an integral of distributed yield force and a linear-spring force. Using a material testing machine, extensive tests (including single-frequency and dual-frequency tests) are conducted to characterize an elastomeric specimen and a linear stroke elastomeric lag damper. The model parameters are determined using a virtual initial loading curve identified from single-frequency force-displacement hysteresis cycles. Efficient numerical algorithms are developed to apply the elastomer model to a dynamic system analysis. The modeling results for single-frequency and dual-frequency damper behavior are correlated quite well with experimental results in a broad-amplitude and moderate-frequency range. This model is successfully applied to predicting the forced response when the specimen is subjected to slowly varying cyclic-loading conditions. It is shown that the nonuniform distributed rate-dependent elastomer model is applicable in complex loading conditions without any prior information, and the flexibility in determining the distribution function provides a potential to improve the model and to apply the model to elastomers with different filler structures.

II. Elastomeric Damper Characterization

To develop an analytical model for the steady-state response of elastomers to harmonic excitation, the behavior of elastomeric dampers must be measured under sinusoidal displacement excitation. In this study, a filled elastomer specimen and an elastomeric lag damper are used, respectively, to characterize the elastomers.

A. Experimental Setup

To characterize elastomeric materials under harmonic excitation, dynamic tests were conducted on two different elastomeric devices. The first elastomeric device was a double-lap-shear specimen, or flat linear bearing, hereinafter called the elastomeric specimen. The second elastomeric device was a linear concentric tubular bearing or damper, hereafter called the elastomeric damper. Testing was carried out with varying excitation amplitudes and frequencies, and all tests were conducted at room temperature (25°C).

A test setup for the elastomeric specimen is shown in Fig. 1 and was designed and built for the purpose of obtaining the elastomeric specimen response data. The silicone-based filled elastomeric

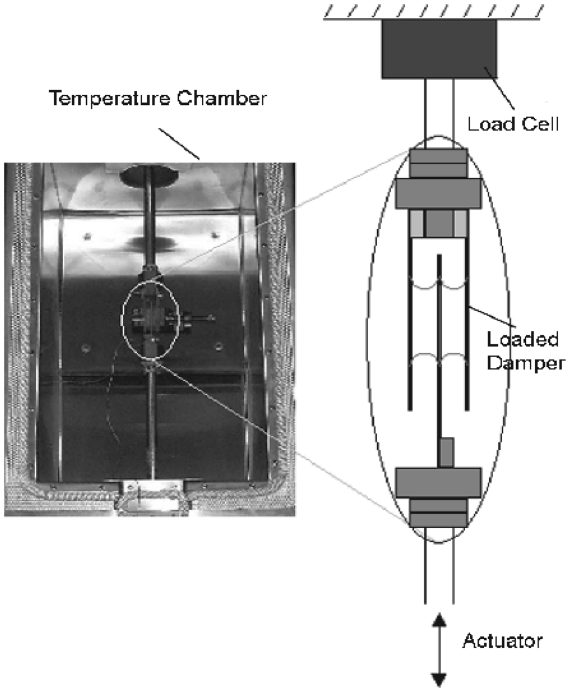

Fig. 1 Elastomeric specimen test setup.

specimen, in the form of double-lap shear, was provided by Paulstra Vibrachoc. As shown in Fig. 2, the specimen has three parallel brass plates between which the elastomeric material is sandwiched symmetrically. To study the effect of preload on damper behavior, the elastomeric specimen tests were conducted using preload and no preload conditions, respectively. The elastomeric specimen was applied preload by compressing the double-lap-shear specimen at 10% of the width of the specimen using a simple vise. A 24.466 kN (5000 lb) servo-hydraulic MTS Systems Corporation test machine was used to test these dampers. Fixtures and grips were designed and machined appropriately to hold the damper specimens in place. A hydraulic power supply unit supplied the servo fluid to the testing machine for power, and the specimen was loaded and tested on the load frame. An actuator on the load frame moved according to the signal sent by a controller. A displacement linear variable differential transformer (LVDT) sensor was used for displacement measurement and a load cell was used for measuring the force. The machine can be operated in two ranges for both displacement ± 127 and ± 12.7 mm

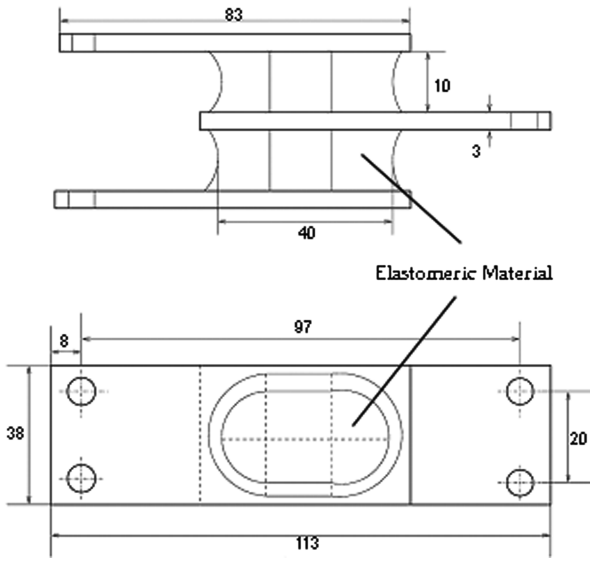

Fig. 2 Schematic of the elastomeric double-lap-shear specimen (dimensions in millimeters).

(± 5 and ± 0.5 in.) and force ± 24.466 and ± 2.4466 kN (± 5000 and ± 500 lb). Single- and dual-frequency tests were conducted by using this machine. In the dual-frequency test, an HP 8904A multifunction synthesizer was used to generate and sum the sinusoidal signals for both frequencies. The single-frequency test was conducted with displacement control for excitation-amplitude range from 0.25 to 5 mm (2.5 to 50% shear) in increments of 0.25 mm. The frequency range was chosen appropriate for a helicopter rotor system: $\Omega_1 = 7.5$ Hz was assumed to be the 1/rev frequency or rotor RPM, $\Omega_{\text{lag}} = 5$ Hz was assumed to be the lag/rev frequency, and $\Omega = 2.5$ Hz was a lower harmonic of these two frequencies. The dual-frequency testing was carried out at 1/rev frequency of $\Omega_1 = 7.5$ Hz and the lag/rev frequency of $\Omega_{\text{lag}} = 5$ Hz. The range of the lag/rev amplitudes were the same as for the single-frequency tests, and the 1/rev amplitudes, respectively, tested were 0.5, 1.5, 2.5, 3.5, and 4.5 mm.

An important effect of filler materials in the filled elastomeric specimen is stress-softening. If an elastomer sample is stretched for the first time to 100% followed by a release in the strain and then stretched again to 200%, there is a softening in the strain of up to 100%, after which it continues in a manner of following the first cycle. This stress-softening effect was first discovered by Mullins and is called the Mullins effect [21]. To account for this phenomenon, the test samples were first cycled and loosened before the actual tests by exciting them at 1-Hz frequency and 5 mm for 300 cycles, because 5 mm is the maximum amplitude during tests. Stress relaxation is also shown in the case of dynamic loading. As the material is subjected to cycling loading, energy dissipation in the material heats up the material and results in high-temperature softening. Usually, material self-heating and other unsteady effects require about 250 s to stabilize and reach a steady state. Hence, to ensure temperature stabilization and consistency of data, during a normal test, the elastomer sample was typically excited at the test frequency and amplitude for 300 s before collecting data. For simplification, the stress-softening and relaxation effects were not considered in the modeling process, such that the distribution function was independent of the loading level and temperature. However, in principle, this model could be used to account for those observed behaviors if the distribution function includes these effects.

A linear concentric tubular elastomeric lag damper was also used to evaluate the performance of the modeling method. The linear stroke elastomeric damper test setup is shown in Fig. 3. As shown in Fig. 4, the elastomeric damper is made of two concentric cylindrical metal tubes and one elastomeric layer sandwiched between an outer and inner tube. The volume enclosed by the inner tube forms a cylindrical inner chamber, and a threaded trapezoidal column is attached to one end of the inner tube. When the damper is installed in the main rotor, the outer tube is attached to the rotor head, and the inner tube is connected to the blade root. Thus, the lead-lag motion of the blade induces a relative translation between the inner tube and the outer tube, which in turn leads to a shear deformation of the elastomer along the damper body length. The deformation of the elastomer provides required stiffness and damping for the lead-lag mode of the

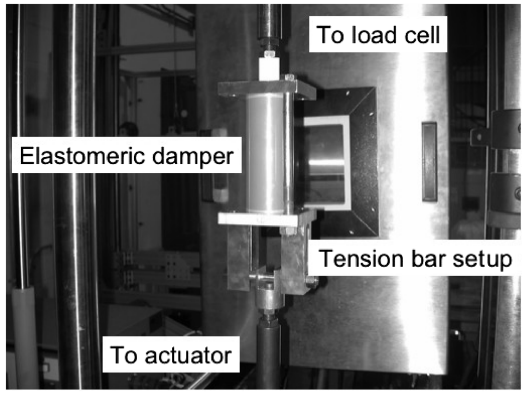

Fig. 3 Elastomeric lag damper test setup.

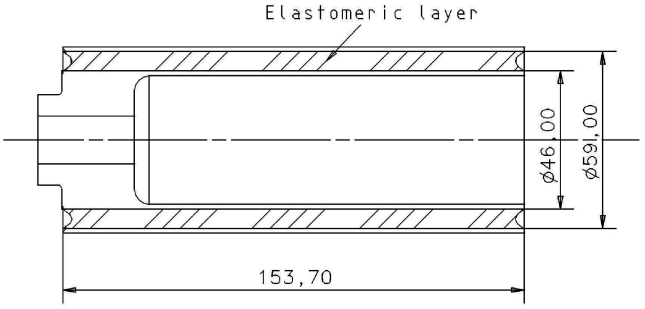

Fig. 4 Cross section of concentric bearing elastomeric lag damper (dimensions in millimeters).

rotor blade. To simulate the loading conditions applied to the elastomeric lag damper by the MTS servo-hydraulic testing machine, the inner tube of the damper was connected with the load cell of the MTS machine by a screw adapter, and the outer tube of the elastomeric damper was connected to the actuator on the MTS loading frame using a tension-rod configuration. Thus, the axial translation of the actuator results in shear deformation of the elastomeric component. The lag damper was excited in displacement control by a sinusoidal signal to simulate damper motion due to the lag motion of a blade. The displacement and force were measured by the LVDT sensor and load cell of the MTS machine. The excitation amplitude ranged from 0.25 mm (10 mil) to 1 mm (40 mil) in increments of 0.25 mm (10 mil) (approximately 5 to 20% shear) at three different frequencies of Ω_1, Ω_{lag}, and Ω_{com}, respectively.

All test data were collected using a high sampling frequency (2048 Hz), such that most higher harmonic components in the measured nonlinear force were included. To reduce the noise of the sinusoidal displacement signal, a Fourier series was used to reconstruct the input displacement. The reconstructed displacement signal was then differentiated to obtain the velocity signal. The Fourier series expansion of the input displacement is

$$x(t) = \frac{x_0}{2} + \sum_{k=1}^{\infty}[X_{c,k}\cos(k\omega t) + X_{s,k}\sin(k\omega t)] \tag{1}$$

where

$$X_{c,k} = \frac{\omega}{\pi}\int_0^{\frac{2\pi}{\omega}} x(t)\cos(k\omega t)\mathrm{d}t \qquad X_{s,k} = \frac{\omega}{\pi}\int_0^{\frac{2\pi}{\omega}} x(t)\sin(k\omega t)\mathrm{d}t \tag{2}$$

For single-frequency data processing, any bias and higher harmonics were filtered so that only the frequency of interest, ω, remained, where $\omega = \Omega$, Ω_{lag}, or Ω_1. For dual-frequency testing, the general equation for the input dual displacement signal is written as

$$x(t) = X_{\text{lag}}\sin(\Omega_{\text{lag}}t) + X_1\sin(\Omega_1 t) \tag{3}$$

The signal is periodic with a frequency corresponding to the highest common factor of both harmonics (i.e., 2.5 Hz in our case). The displacement signal was filtered using $\Omega = 2.5$ Hz as the base frequency. The first three harmonics were needed to reconstruct the dual-frequency displacement signal to capture the lag/rev and the 1/rev frequencies. The Fourier series was also used to reconstruct the measured force. However, due to nonlinearity of elastomers, the higher harmonics of the measured force were not filtered.

B. Damper Characterization

A typical approach used for characterizing elastomer behavior is the complex stiffness. The linearized complex stiffness K^* is composed of an in-phase or storage stiffness K' and a quadrature or loss stiffness K'', as follows:

$$K^* = K' + jK'' \tag{4}$$

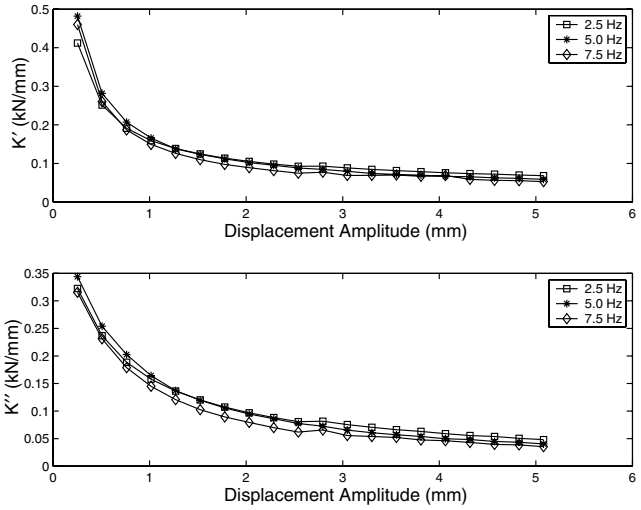

Fig. 5 Linear characterization of an elastomeric specimen.

Therefore, the damper force can be written as the summation of an in-phase spring force and a quadrature damping force, and the damper force can be approximated by the first Fourier sine and cosine components at the frequencies $\omega = \Omega$, Ω_{lag}, and Ω_1:

$$F(t) = F_c\cos(\omega t) + F_s\sin(\omega t)$$
$$F(t) = K'x(t) + \frac{K''}{\omega}\dot{x}(t) \tag{5}$$

where F_c and F_s are the first harmonic Fourier coefficients of the measured force. The storage stiffness K' and the loss stiffness K'' are determined by the following equations:

$$K'(\omega) = \frac{F_cX_c + F_sX_s}{X_c^2 + X_s^2} \qquad K''(\omega) = \frac{F_cX_s - F_sX_c}{X_c^2 + X_s^2} \tag{6}$$

where X_c and X_s are the first harmonic Fourier coefficients of $x(t)$.

The typical linear characterization results of the elastomeric specimen are shown in Fig. 5, in which no preload was applied to the elastomeric specimen. These plots indicate that the linearized storage stiffness and loss stiffness of the specimen are highly amplitude-dependent at low amplitudes. For smaller amplitudes, the rate of change of the storage stiffness and the loss stiffness is much greater than that for larger amplitudes. However, the complex stiffness does not change substantially over the narrow frequency range tested. The loss factor η is also strongly dependent on amplitude. The maximum value of the loss factor is as high as 1.025 for this filled elastomer. This is much higher than the values for existing lag damper materials. This elastomeric material performs most effectively within the amplitude range of 0.76–1.27 mm (7.5 to 12.5% shear strain), where the loss factor $\eta > 1$. Similar results are demonstrated by the elastomer with preload. Thus, it can be concluded that the linearized behavior of the elastomeric specimen is highly amplitude-dependent and weakly frequency-dependent in this frequency range.

The measured complex modulus and loss factor of the elastomeric lag damper are shown in Fig. 6. Both in-phase and quadrature stiffness demonstrate moderate amplitude dependence and weak frequency dependence. In contrast to the characteristics of the elastomeric specimen, the in-phase stiffness of the elastomeric damper is much higher than the quadrature stiffness, and both in-phase and quadrature stiffness vary with the displacement amplitude at a similar rate. Thus, the loss factor of the elastomeric damper is quite low (around 0.25 to 0.3) and almost constant along different displacement amplitudes and frequencies, as shown in Fig. 6b.

The single-frequency linear characterization can capture the general trends of the in-phase and quadrature stiffness for a filled elastomer. However, this linear analysis cannot be used to accurately reconstruct the nonlinear hysteresis behavior exhibited by the elastomer [6]. Therefore, a new nonlinear modeling effort will be presented in the following section.

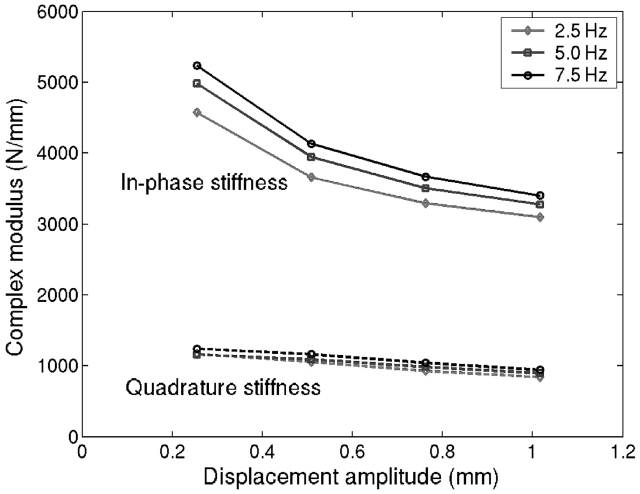

a) Complex modulus

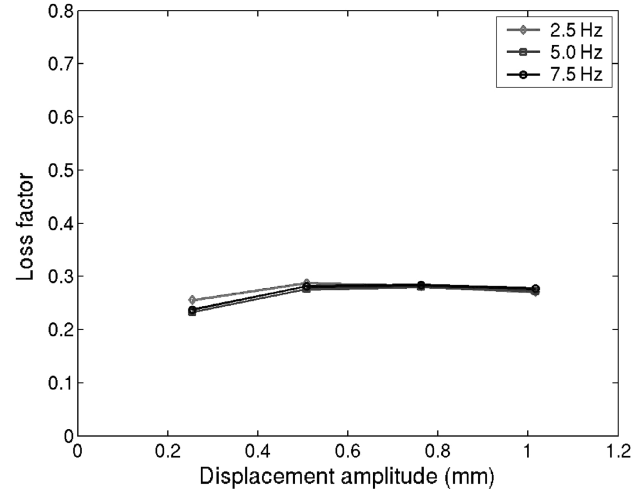

b) Loss factor

Fig. 6 Linear characterization of the elastomeric damper.

III. Distributed Rate-Dependent Elastoslide Model

A. Model Development

The distributed rate-dependent elastoslide model is shown in Fig. 7, in which a series of elastoslide elements is combined in parallel with a constant linear spring. The model can be applied either in force-displacement relations or in stress–strain relations, but only the force-displacement formulation will be used in this study. Each elastoslide element consists of a leading spring with stiffness k/N in series with a slide that has a yield force f_i^*/N, where N is the total number of elements. The yield force for each element is different, and the stiffness for each leading spring is assumed to be a constant. The ideal model assumes that the yield force is a Coulomb force, which is a constant as the slide moves at any speed. However, the rate-dependent elastoslide model represents real friction behavior by representing the yield force of the slide as a function of the slide velocity. This function will be discussed later. For simplicity, the description of the model starts from using an ideal slide (which has an ideal Coulomb force), and then the behavior of the model will be studied when the ideal slide is replaced by a rate-dependent slide.

First, we will apply a displacement x to the ideal elastoslide element, which assumes a constant Coulomb force. At the beginning of the displacement, x is small, such that the consequent leading spring force is smaller than the yield force, and so only the spring is deformed. After the spring force reaches the yield force, the slide yields and a motion is induced, and the resisting force of the element remains constant with the same value as the yield force. Because each elastoslide element in the model is assumed to have a different yield-force level, this model shows gradual stiffness reduction as amplitude increases, until all elements have yielded. At that time, only the parallel spring k_0 remains to represent the polymer stiffness of the elastomer. Because the elastomer is a continuum, the total number of elements N approaches infinity, and in the limit, the discrete yield force for a single slide is replaced by a distributed density within a certain yield-force range. Alternatively, a mathematically equivalent model is shown in Fig. 8, in which f_e represents the total resisting force of the elastoslide elements.

The following simulation using the model will show that the existence of the filler structures inside the elastomer can lead to hysteretic behaviors when the damper is cycled between fixed deflection limits. Analytically, a distribution function of the yield force is denoted as $\varphi(f^*)$, such that the density of the slides with yield force f^* is expressed as $\varphi(f^*)\mathrm{d}f^*$. Using the ideal slide assumption, the slide behaves as a Coulomb friction element. Thus, upon initial loading, the leading spring at a certain yield element stretches with the displacement x until the spring force reaches the maximum slide yield force; that is,

$$\begin{aligned} \mathrm{d}f &= kx\varphi(f^*)\mathrm{d}f^* \qquad \dot{x} > 0 \qquad 0 \leqslant x \leqslant \frac{f^*}{k} \\ \mathrm{d}f &= f^*\varphi(f^*)\mathrm{d}f^* \qquad \dot{x} > 0 \qquad x \geqslant \frac{f^*}{k} \end{aligned} \tag{7}$$

If the direction of loading is reversed, the force-deflection relation is more complicated. Including the yielded and not-yielded elements, the force-deflection relation becomes

$$\begin{aligned} \mathrm{d}f &= [f^* - k(A-x)]\varphi(f^*)\mathrm{d}f^* \qquad \dot{x} < 0 \\ & A - 2\frac{f^*}{k} \leqslant x \leqslant A \qquad f^* \leqslant kA \\ \mathrm{d}f &= -f^*\varphi(f^*)\mathrm{d}f^* \qquad \dot{x} < 0 \qquad x \leqslant A - 2\frac{f^*}{k} \qquad f^* \leqslant kA \\ \mathrm{d}f &= kx\varphi(f^*)\mathrm{d}f^* \qquad \dot{x} < 0 \qquad f^* > kA \end{aligned} \tag{8}$$

where A is the maximum deflection that occurred with $\dot{x} > 0$. An expression similar to Eq. (8) is obtained when the loading reaches the minimum deflection and is reversed again so that $\dot{x} > 0$. This process

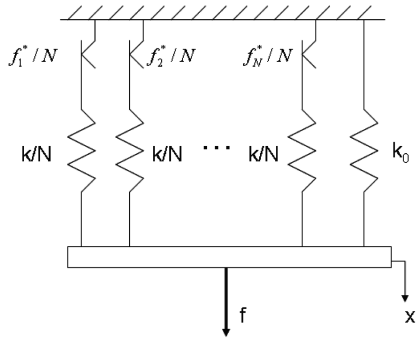

Fig. 7 Distributed elastoslide model.

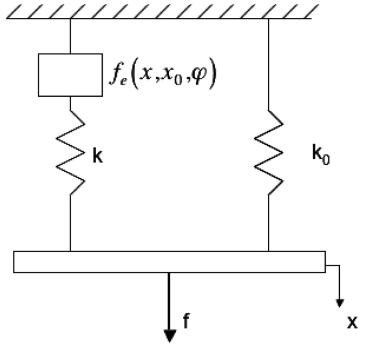

Fig. 8 Mathematically equivalent elastomer model.

continues until the loading is terminated. Clearly, at each time, only some of the elastoslide elements have yielded. The total resisting force can be obtained by integrating all of the elastoslide forces along the yield-distribution region and by adding the spring force due to the residual polymer stiffness. From Eq. (7), the initial loading force is given as

$$f = \int_0^{kx} f^*\varphi(f^*)\mathrm{d}f^* + kx\int_{kx}^{\infty}\varphi(f^*)\mathrm{d}f^* + k_0x, \qquad \dot{x} > 0 \quad (9)$$

Similarly, the resisting force due to the reversed loading is obtained by integrating Eq. (8):

$$f = \int_0^{\frac{k(A-x)}{2}} -f^*\varphi(f^*)\mathrm{d}f^* + \int_{\frac{k(A-x)}{2}}^{kA}[kx-(kA-f^*)]\varphi(f^*)\mathrm{d}f^* + kx\int_{kA}^{\infty}\varphi(f^*)\mathrm{d}f^* + k_0x$$
$$\dot{x} < 0 \qquad x \leqslant A \quad (10)$$

Thus, while an elastomer is under the cyclic displacement loading,

$$x = A\sin(\omega t) \quad (11)$$

A theoretical force-deflection hysteresis cycle is shown as a dashed line in Fig. 9, in which A is 2.5 mm and the frequency is 2.5 Hz. Compared with the experimental hysteresis shown as a dotted line, the model prediction gives a good match to the experimental result.

The distributed elastoslide model resembles the physical mechanism of an elastomer so that it can account for nonlinear characteristics of the behavior demonstrated by the elastomer under a cyclic loading either in single-frequency or multiple frequencies. However, using the ideal slide with a Coulomb force, the cyclic displacement limit at turning points must be known for response calculation, which makes it impossible for the model to describe elastomer behavior under complex loading conditions. The ideal elastoslide is also incapable of modeling frequency-dependent properties and nonhysteretic behavior in the time domain, such as stress relaxation or creep. In reality, the Coulomb slide is only an idealized friction model. The practical friction behavior includes a preyield slip and a postyield steady resistances which leads to a rate-dependent damping effect [22,23]. Thus, a rate-dependent elastoslide model is introduced to improve the modeling performance.

In the rate-dependent elastoslide model, the Coulomb slide is replaced with a non-Coulombic friction function and the coupling between a slide and a leading spring is described by an internal displacement denoted as x_0, such that the slide force at a certain yield region is written as

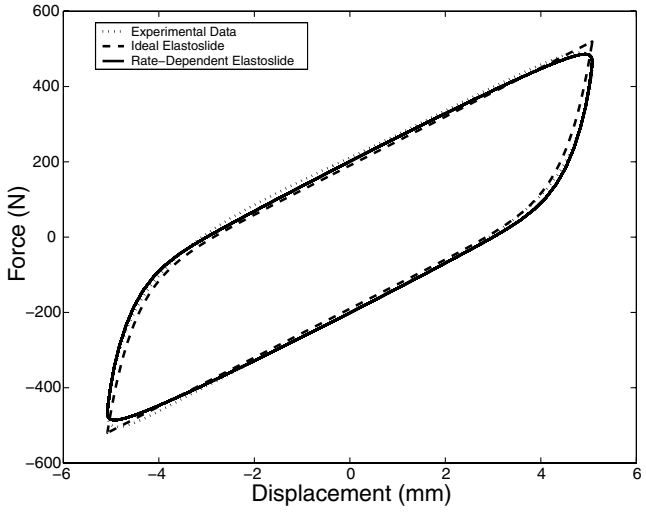

Fig. 9 Hysteresis modeling for elastomeric specimen.

$$\mathrm{d}f = f^*\varphi(f^*)\mathrm{d}f^*\left(\frac{\dot{x}_0}{v_r}\right)^{\frac{1}{p}} \quad (12)$$

where p is a positive odd integer and v_r is a yield transition velocity. Coupled with the lead spring $k\varphi(f^*)\mathrm{d}f^*$, the internal displacement x_0 at a certain yield region is obtained using the function

$$\frac{\dot{x}_0}{v_r} = \left[\frac{k}{f^*}(x-x_0)\right]^p \quad (13)$$

By integration over the whole yield-force region, the total force due to the elastoslide element is obtained as

$$f_e = \int_0^{\infty} k(x-x_0)\varphi(f^*)\mathrm{d}f^* \quad (14)$$

Adding the spring force due to the polymer stiffness, the damper force due to any deflection loading, x, is determined by

$$f = f_e + k_0x = \int_0^{\infty} k(x-x_0)\varphi(f^*)\mathrm{d}f^* + k_0x \quad (15)$$

This relation can be shown in Fig. 8. Equation (13) is a typical well-posed initial-value problem, and numerical solution for this differential equation can be obtained given an initial condition. The simplest way to guarantee a stable solution for the problem is to adopt a predictor–corrector, or more precisely, a predictor-evaluate–corrector-evaluate (PECE) method, with the corrector iterated to convergence [24]. In this application, the numerical algorithm is based on the Adams–Bashforth four-step method as the predictor step and one iteration of the Adams–Moulton three-step method as the corrector step, with the starting values obtained from a Runge–Kutta method of order four. In accordance with the ratio of the yield force and the stiffness, k/f^*, and an appropriate choice of p, the Adams–Bashforth–Moulton method gives relatively stable and fast convergence of a solution within a limited number of e steps.

For an elastomer under loading, as in Eq. (11), the steady-state response predicted by the rate-dependent elastoslide model is shown as the solid line in Fig. 9. The predicted hysteresis cycle correlates much better with the experimental data, especially at turning points of the loading deflection. It should be noted that there is no requirement for excitation amplitude information in this modeling process. Thus, the distributed rate-dependent elastoslide model can predict time-domain-forced response of an elastomer under a sinusoidal displacement excitation.

To apply the elastomer model to a dynamic system, a numerical method using a MATLAB ordinary differential equation (ODE) algorithm was also evaluated. For a dynamic system with a governing equation,

$$M\ddot{x} + C\dot{x} + Kx + F_d(x,\dot{x}) = F(t) \quad (16)$$

where M, C, and K are the mass matrix, equivalent damping matrix, and stiffness matrix, respectively; $F_d(x,\dot{x})$ is used to describe the force due to an elastomeric damper; and $F(t)$ is a loading vector applied to the system. The size of the matrix depends on the degrees of freedom of the system. For simplicity, only a 1-DOF system is considered now. In the distributed rate-dependent elastoslide damper model, there are theoretically an infinite number of internal variables x_0. However, the distributed yield stress usually falls within a limited range. Therefore, according to the form of a distribution function, the continuous yield-force distribution area can be uniformly decomposed into n discrete elements from minimum to maximum yield force and each element has a yield-force range Δf^*. At each yield stress f_i^*, the corresponding distribution is equal to the area of that element, $\varphi(f_i^*)\Delta f^*$. Thus, each element has an internal variable denoted as x_{0i} $(i = 1, \ldots, n)$, and each x_{0i} satisfies Eq. (13). Thus, the damper force F_d can be described by

$$F_d = k\sum_{i=1}^{n}\varphi(f_i^*)\Delta f^*(x-x_{0i}) + k_0x \quad (17)$$

Rewriting Eq. (16) into a first-order form and combining Eqs. (13) and (17), the state equation of the system is expressed as

$$\dot{x} = \dot{x}$$

$$\ddot{x} = \frac{F(t)}{M} - \frac{1}{M}\left[(K + k_0)x - k\sum_{i=1}^{n}\varphi(f_i^*)\Delta f^*(x - x_{0i})\right] - \frac{C}{M}\dot{x}$$

$$\dot{x}_{01} = \left[\frac{k}{f_1^*}(x - x_{01})\right]^p v_r \tag{18}$$

$$\vdots$$

$$\dot{x}_{0n} = \left[\frac{k}{f_n^*}(x - x_{0n})\right]^p v_r$$

This is a $(n + 2)$th-order state function. Using the ODE23 algorithm in MATLAB, the forced response due to $F(t)$ or/and the transient response due to the initial conditions $x(0)$ and $\dot{x}(0)$ can be solved numerically. For the system with more degrees of freedom or elastomeric dampers, the state function can easily accommodate these additions by using a larger number of states.

B. Model Parameters Determination

As seen in the construction of the model, the major parameters to be determined are the leading spring k and yield-force distribution function $\varphi(f^*)$ for the distributed elastoslide element and the parallel spring k_0 for the remaining polymer stiffness. In the absence of the knowledge of the elastomer structure, the selection of these parameters is only based on experimental data in this stage. One possible selection of methods would be to make use of an experimentally determined initial loading curve.

The definition of the distribution function implies that $\varphi(f^*)$ has to obey the following three constraints:

$$\int_0^\infty \varphi(f^*)\mathrm{d}f^* = 1 \qquad \varphi(f^*) \geqslant 0 \qquad 0 \leqslant f^* \leqslant \infty \tag{19}$$

The initial loading curve, Eq. (9), yields

$$\frac{\mathrm{d}f}{\mathrm{d}x} = k\int_{kx}^\infty \varphi(f^*)\mathrm{d}f^* \tag{20}$$

where

$$f^* = kx \tag{21}$$

Then

$$\frac{\mathrm{d}^2 f}{\mathrm{d}x^2} = -k^2\varphi(f^*) \tag{22}$$

Thus, the distribution function would be related to the curvature of the initial loading curve by the following formula:

$$\varphi(f^*) = -\frac{1}{k^2}\frac{\mathrm{d}^2 f}{\mathrm{d}x^2} \tag{23}$$

And the determination of the distribution function relies on the identification of the initial loading curve from the experimental data.

In view of the distributed elastoslide model using an ideal Coulomb slide, the initial loading curve is independent of loading rate, such that the maximum force in the initial loading curve responds to the maximum displacement in cyclic loading, as seen in Eq. (9). As a result, an initial loading curve can be obtained using a series of experimental hysteresis loops at different amplitudes. An example of the initial loading curve is shown in Fig. 10: the initial loading curves at three different frequencies are obtained from hysteresis cycles of the elastomeric specimen by identifying the force at corresponding maximum displacements. The analytical initial loading curve is determined by considering the influence of the rate-dependent slide. This curve exhibits elastoplastic behavior, which is described as

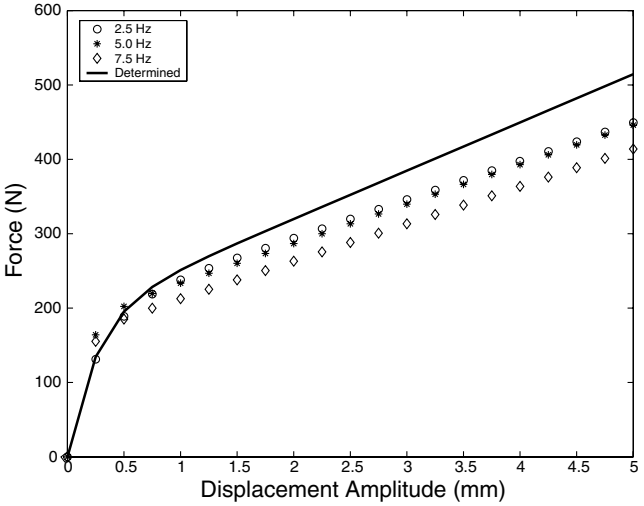

Fig. 10 Determination of the initial loading curve for elastomeric specimen.

$$f = \frac{1}{\varphi_0}(1 - e^{-k\varphi_0 x}) + k_0 x \tag{24}$$

Notably, φ_0 is a distribution constant and an index of the postyield-force level, and k and k_0 are the stiffness of the leading spring and the remaining polymer stiffness, respectively. Summation of the leading spring and the polymer stiffness is just the slope of the force-displacement curve when $x \to 0$. This is conceivable because the influence of the springs only exists when all slide elements are not yielded. Substituting Eq. (24) into Eq. (23) yields a very simple distribution function as

$$\varphi(f^*) = \varphi_0 e^{-\varphi_0 f^*} \tag{25}$$

The distribution area for the elastomeric specimen is shown as the area below the curve in Fig. 11. It is easily shown that the distribution function satisfies all the properties of Eq. (19).

After φ, k, and k_0 are determined for the distributed elastoslide model using a Coulomb slide, the steady-state forced response of the damper under cyclic loading will be predicted as follows:

$$\begin{aligned} f &= \frac{1}{\varphi_0}(1 + e^{-k\varphi_0 x_{\max}} - 2e^{-k\varphi_0\frac{x - x_{\min}}{2}}) + k_0 x \qquad \dot{x} > 0 \\ f &= -\frac{1}{\varphi_0}(1 + e^{-k\varphi_0 x_{\max}} - 2e^{-k\varphi_0\frac{x_{\max} - x}{2}}) + k_0 x \qquad \dot{x} < 0 \end{aligned} \tag{26}$$

where $x_{\max}$ and $x_{\min}$ are the displacement at turning points when $\dot{x} < 0$ and $\dot{x} > 0$, respectively.

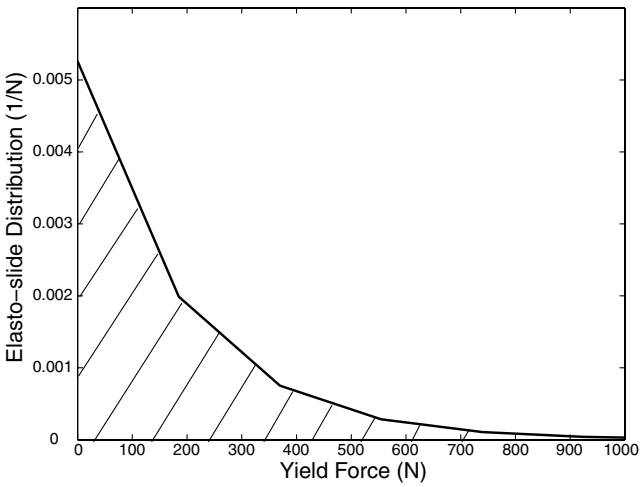

Fig. 11 Elastoslide distribution for elastomeric specimen.

Table 1 Model parameters for the elastomeric specimen

Parameter	No preload	10% preload
φ_0, 1/newton	0.0068	0.0053
k, N/mm	504.51	739.40
k_0, N/mm	44.44	64.87
v_r, mm/s	50	50
p	7	7

Table 2 Model parameters for elastomeric damper

Parameter	No preload
φ_0, 1/newton	0.0015
k, N/mm	6436
k_0, N/mm	2915
v_r, mm/s	15
p	7

For the rate-dependent elastoslide model, the reference velocity v_r and the exponent p need to be determined. The choice of v_r is based on steady-state force-velocity curves in which the boundary between the preyield and postyield region is approximated. Analytically, p should be as large as possible, such that the postyield force rapidly transitions to a constant value, which is similar to friction behavior. However, large values of p result in a stiffer system. Thus, p was chosen by a tradeoff between both factors. For the elastomeric specimen, the determined model parameters are shown in Table 1, in which the elastomeric damper has two preload conditions. Notably, the distribution constant φ_0 at 10% preload is lower than that without preload. This means that the yield-force level can be increased by the normal force in the preload condition. Similarly, the preload force also can increase the stiffness. As a result, the addition of a preload perpendicular to the loading axis tends to increase the equivalent stiffness and damping over the entire amplitude range. This effect is due to the compressive preload increasing the friction response of the filler in the elastomer and is not reflected in the distributed elastoslide model. Thus, the model parameters are different for different preloading conditions. For the elastomeric lag damper, the determined model parameters are shown in Table 2. Notably, the elastomeric material in the elastomeric damper is much stiffer than the elastomeric specimen, because the stiffness of the leading spring and remaining spring is much higher than the elastomeric specimen. Thus, the loss factor of the elastomeric damper appears much lower than the elastomeric specimen, though the yield-force level of the elastomeric damper is higher than the elastomeric specimen.

IV. Modeling Results and Validations

As stated before, the distributed rate-dependent elastoslide model resembles the behavior of filler structures in the elastomer, such that it can predict the forced response of an elastomer in the time domain. In this section, single-frequency and dual-frequency steady-state hysteresis data are used to evaluate the fidelity of the model, in which the model is validated over an amplitude and frequency range appropriate for helicopter lag dampers. Because the intention is to apply these materials in a lag damper in a helicopter rotor, the damper response under dual-frequency loading with slowly varying amplitude is also correlated with model predictions.

A. Single-Frequency Modeling Results

For the elastomeric specimen, three sets of single-frequency hysteresis cycle data are used to verify the fidelity of the analysis. Each set of data is obtained by measuring the forced response while the elastomeric specimen is under sinusoidal displacement excitation at 2.5, 5.0, and 7.5 Hz, respectively. At each frequency, the loading amplitude is chosen as 1, 2, 3, and 4 mm. In Figs. 12a–12c, the experimental data at three frequencies are shown compared with the modeling results. Basically, the modeling results correlate quite well with the experimental results, whereas the displacement amplitude x_0 is in the moderate-amplitude range ($2 < x_0 < 5$ mm). In the small-amplitude range $x_0 < 2$ mm, the elastomer model underpredicts the area enclosed by the hysteresis cycle. The reason for that is partly because the lower yield region for the elastoslide element is replaced

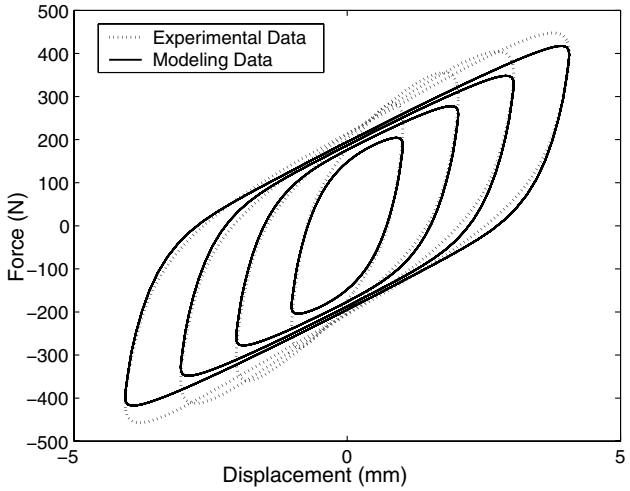

a) 2.5 Hz

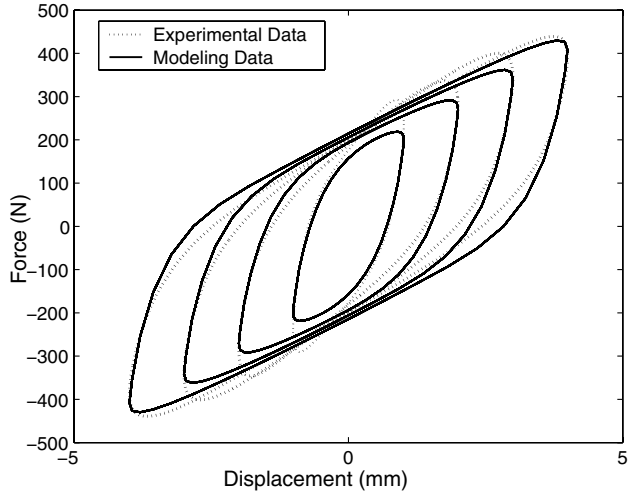

b) 5.0 Hz

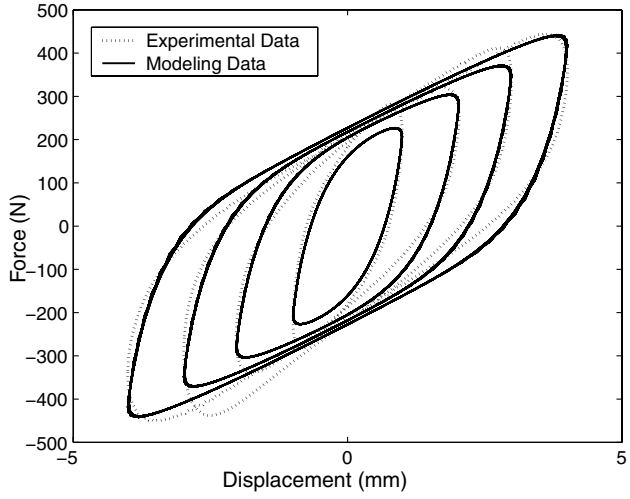

c) 7.5 Hz

Fig. 12 Single-frequency hysteresis modeling for elastomeric specimen.

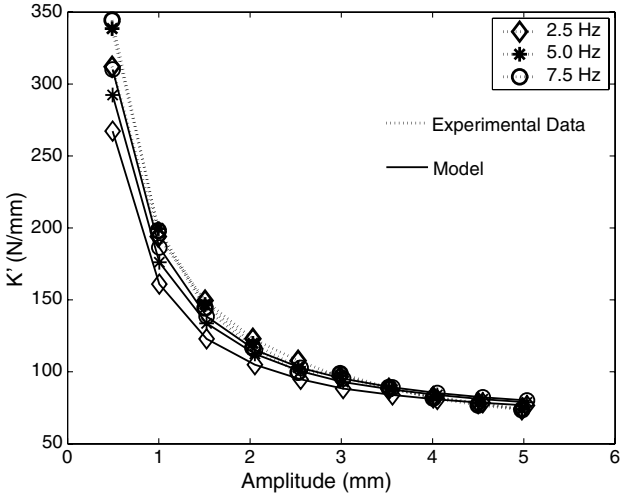

a) In-phase stiffness

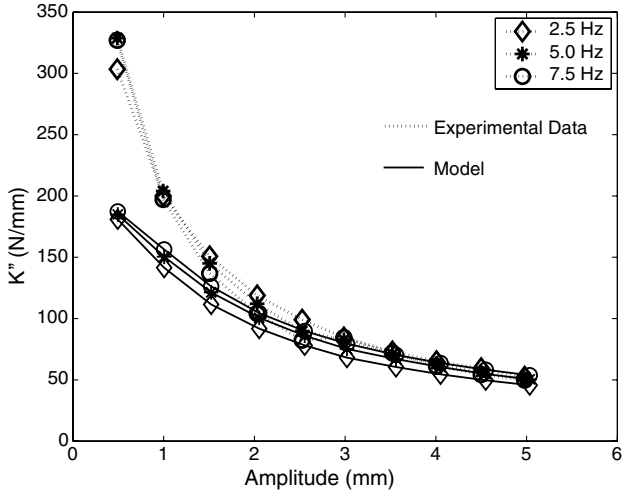

b) Quadrature stiffness

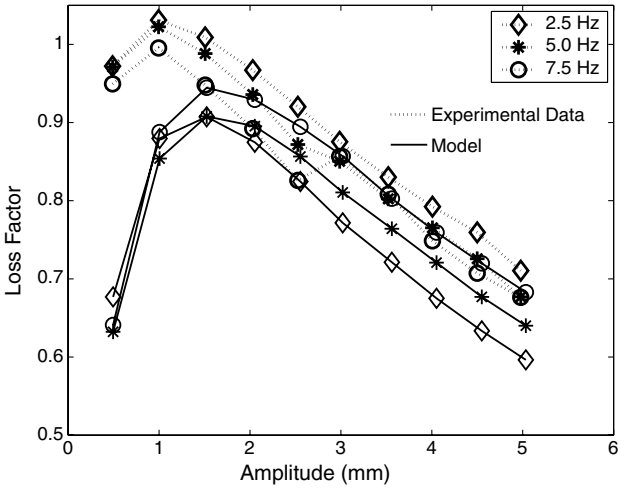

c) Loss factor

Fig. 13 Variation of complex modulus with dynamic amplitude for elastomeric specimen.

with a nonzero constant yield force for numerical consideration and the influence of this approximation is amplified at small-deflection loading.

The complex modulus determined by the elastomeric model is also compared with the experimental result. As shown by solid lines in Fig. 13, the storage stiffness and loss stiffness predicted by the model have the same amplitude-dependent trend as the experimental result. The experimental moduli are well-matched by the analytical moduli at moderate-amplitude range, except that the moduli over small-amplitude range are underpredicted, especially for loss stiffness. Model predictions are also compared with experimental data for loss factor. The predicted loss factor shares common features of the elastomer. Clearly, at small amplitude, most of the filler structures or corresponding elastoslide elements have not yielded, and so the loss

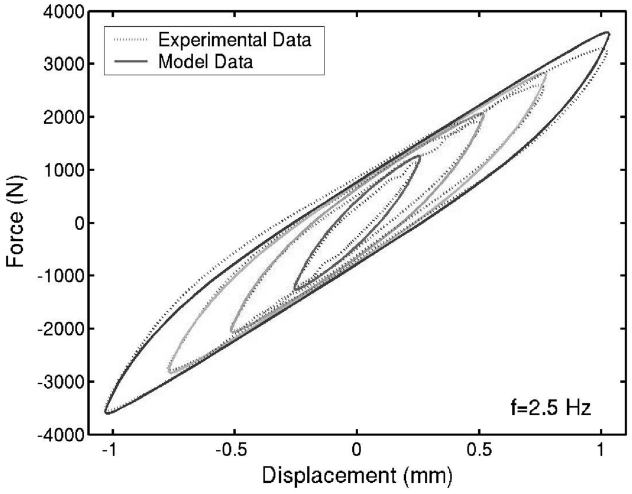

a) 2.5 Hz

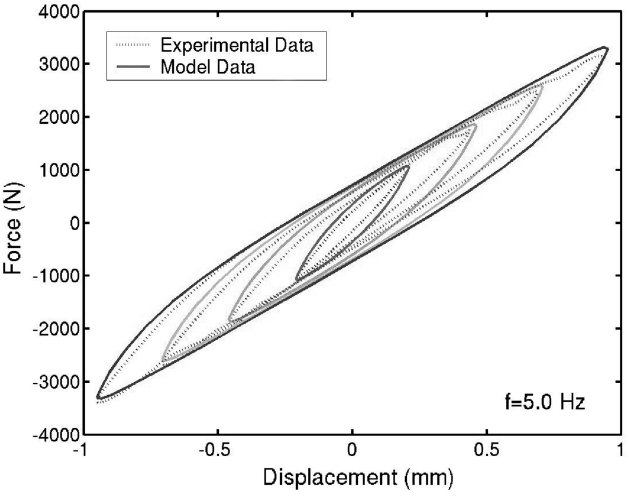

b) 5.0 Hz

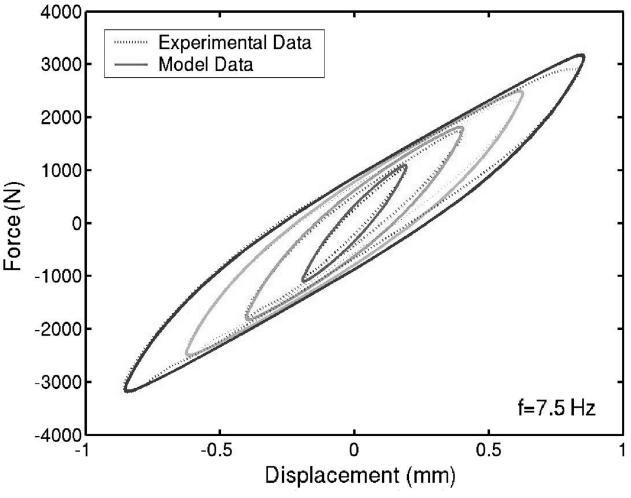

c) 7.5 Hz

Fig. 14 Single-frequency hysteresis modeling for elastomeric damper.

factor is small. As the amplitude increases, breaking filler structures or yielding of slides leads to a rise in the loss factor. After all of the slide elements have yielded, the loss factor decreases again. Fig. 13 also shows that both experimental and predicted moduli are weakly dependent on frequency. This phenomenon is consistent with the triboelastic mechanism of elastomeric materials [20].

Similar single-frequency modeling results for the elastomeric lag damper are shown in Fig. 14 as force-displacement diagrams for different amplitudes at 2.5 Hz (Fig. 14a), 5 Hz (Fig. 14b), and 7.5 Hz (Fig. 14c), respectively. Clearly, the elastomeric model captures the amplitude- and frequency-dependent behavior of the elastomeric damper.

B. Dual-Frequency Modeling Results

In a helicopter lag damper, the elastomer would experience multifrequency excitation, especially as a combination of regressive lead-lag frequency and 1/rev rotor frequency, while the helicopter is in the forward-flight condition. Under such a circumstance, the potential loss of damping at the lag frequency due to limitation of stroke is well-known [3], and so it is important to predict the response of the elastomeric dampers under dual-frequency excitation. Experimental dual-frequency force-displacement data of the elastomeric specimen are used to evaluate the adaptability of the model under complex loading conditions.

In a steady-state forward-flight condition, the blade motion at 1/rev is constant at a given amplitude. Thus, the test data were obtained while the amplitudes at both frequencies (lag/rev and 1/rev) were held constant. For each test condition, the amplitude for lag frequency and 1/rev frequency ranged from 0.25 to 5 mm, and the sum of both amplitudes must not exceed 5 mm, which corresponds to the maximum allowable strain of 50%. The modeling result at each dual-frequency loading condition is correlated with the corresponding experimental result. Some of these dual-frequency modeling results are presented in Figs. 15 and 16. The figures are grouped according to the 1/rev frequency amplitude. Figure 15 shows the modeling results for 2.5-mm amplitude at the 1/rev frequency and at four different amplitudes at lag frequency. Because the displacement amplitude at 1/rev is 2.5 mm, the experimental dual-frequency behavior can be matched quite well by the elastomer model. Comparatively, Fig. 16 shows the modeling results for 0.5-mm amplitude at the 1/rev frequency and at four different amplitudes at lag frequency. Notably, the model underpredicts the forced response as the total amplitude at lag/rev, and 1/rev is below 2.5 mm because the high yield-force region in Fig. 11 is not well-described by the numerical algorithm of the model. In general, the distributed rate-dependent elastoslide model performs well in the moderate-amplitude range, except it overpredicts the inner loop in some cases. The model also should be improved to predict the response over the small-amplitude range.

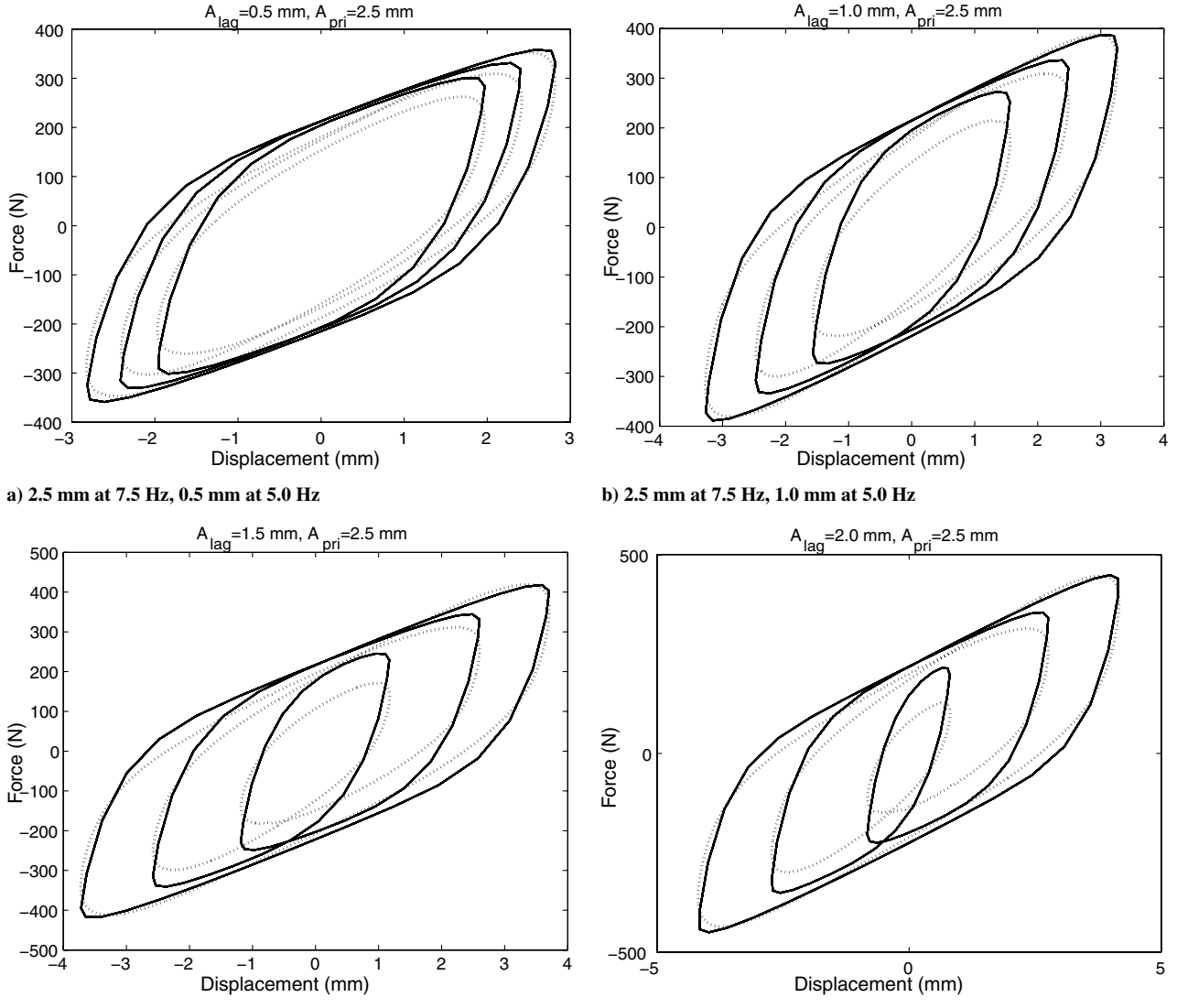

a) 2.5 mm at 7.5 Hz, 0.5 mm at 5.0 Hz

b) 2.5 mm at 7.5 Hz, 1.0 mm at 5.0 Hz

c) 2.5 mm at 7.5 Hz, 1.5 mm at 5.0 Hz

d) 2.5 mm at 7.5 Hz, 2.0 mm at 5.0 Hz

Fig. 15 Dual-frequency hysteresis modeling for elastomeric specimen.

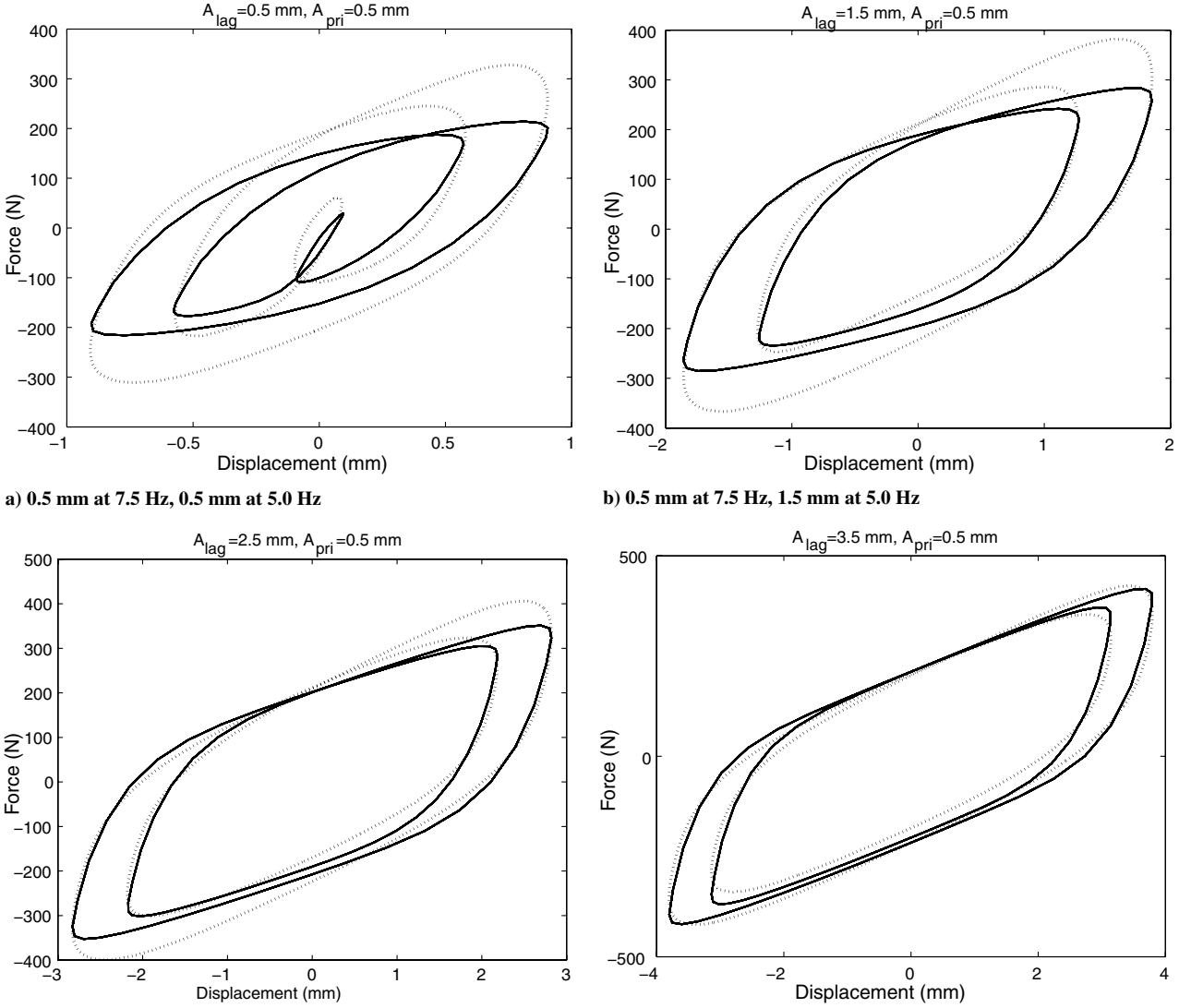

a) 0.5 mm at 7.5 Hz, 0.5 mm at 5.0 Hz

b) 0.5 mm at 7.5 Hz, 1.5 mm at 5.0 Hz

c) 0.5 mm at 7.5 Hz, 2.5 mm at 5.0 Hz

d) 0.5 mm at 7.5 Hz, 3.5 mm at 5.0 Hz

Fig. 16 Dual-frequency hysteresis modeling for elastomeric specimen.

In transient forward-flight conditions such as those due to air turbulence, the lead-lag damper may encounter a slowly varying amplitude-modulated periodic loading. For simplicity, the analytical and experimental simulation results are only shown for one scenario, in which the amplitude for 1/rev frequency is 1.5 mm and the amplitude for lag frequency is assumed as

$$A_{\text{lag}} = 1.5[1 + 0.2\sin(0.2\pi t)] \text{ (mm)} \tag{27}$$

The predicted forced response is shown in Figs. 17a and 17b and compared with the experimental results for two different time scales. Similarly, the modeling force-displacement hysteresis cycle is also compared with the experimental data, as shown in Fig. 17c. As seen, the predicted damper response due to the slowly varying displacement excitation exhibits the same varying trend as the real damper behavior, and the force value is also tracked quite well. Clearly, the proposed elastomeric model performs fairly well in predicting dual-frequency response and, especially, the distributed elastoslide model can predict the behavior of the elastomeric damper under slowly varying amplitude-modulated periodic loadings.

V. Conclusions

Modeling methods for describing elastomeric material behavior were investigated. Most earlier models introduced nonlinear terms into the conventional Kelvin model or Zener model. Because filled elastomers are anelastic materials, a friction-mechanism-damping element proves useful to model rate-independent damping. Nonlinearity in tested elastomeric materials manifested in two ways. First, the forced response of an elastomer under cyclic loading was nonlinear (nonelliptical), which meant that the response could not be predicted by linear differential or integral equations. Second, stiffness and damping of elastomers vary as functions of amplitude and frequency. Therefore, different modeling emphases result in different model effectiveness. Although some models capture the amplitude-dependent complex moduli very well with constant parameters, they cannot predict stress–strain or force-displacement hysteresis accurately. On the other hand, most hysteresis models can predict nonelliptical hysteresis quite well, but their parameters are usually amplitude- and frequency-dependent. The methods require amplitude and frequency as prior information when these models are implemented.

Based on a hysteresis modeling method, a distributed rate-dependent elastoslide elastomeric model was used to describe the amplitude-dependent characteristics of an elastomer. This physically motivated damper model resembles the behavior of filler structures in the elastomer under cyclic loading. A method to determine the model parameters was presented. It was found that a unique exponential function can be used to describe the yield-force distribution for elastomers. Numerical algorithms were developed for model applications. Dynamic tests were conducted on a double-lap-shear elastomeric specimen and on a linear, concentric-tube, elastomeric

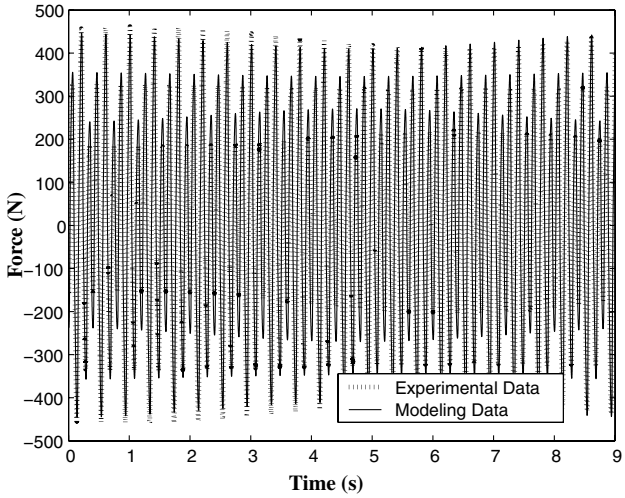

a) Forced response (0-9 Seconds)

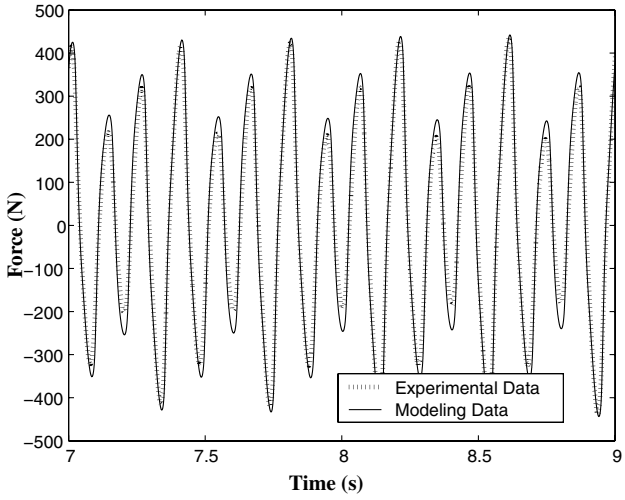

b) Forced response (7-9 Seconds)

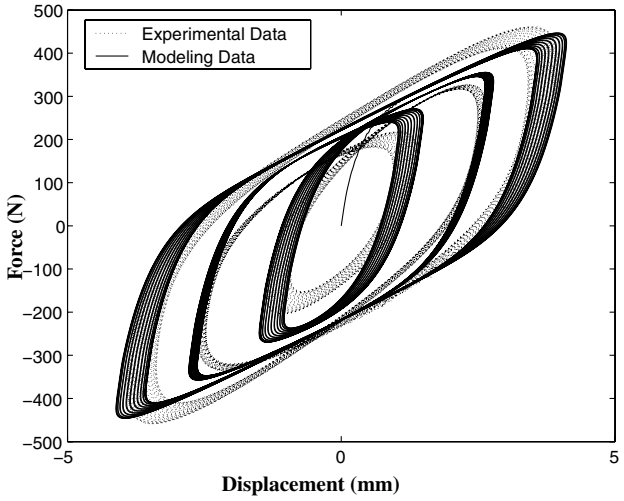

c) Force-displacement hysteresis

Fig. 17 Modeling results for dual frequency with slowly varying amplitude.

bearing, respectively, and the test results were used to evaluate the modeling method. The fidelity of the model was verified by the good correlation between the predicted single- and dual-frequency force-displacement hysteresis and the experimental results, except that the damping at lower-amplitude range cannot be fully predicted by the model. Because the proposed model is a time-domain model, the adaptability of the model in predicting damper response under a slowly varying displacement excitation was evaluated. The predicted force response of the elastomeric specimen under this slowly varying displacement excitation correlated quite well with the corresponding experimental data.

In conclusion, the distributed rate-dependent elastoslide elastomeric damper model is a time-domain modeling approach to capture nonlinear behavior of the elastomer. The damper model, formulated as a state-space model, has the advantage that it can easily be implemented into dynamic system models such as helicopter rotor analyses. Because the model is physically motivated, the flexibility in determining the distribution function provides means to improve the model performance, especially over the low-amplitude range. Although only a one-dimensional elastomeric model is described in this paper, the distributed elastoslide model can also be extended into a three-dimensional form, such that it can be implemented easily into a finite element analysis for a complex elastomeric damper configuration.

References

[1] Coveney, V. A., Johnson, D. E., and Turner, D. M., "A Triboelastic Model for the Cyclic Mechanical Behavior of Filled Vulcanizates," *Rubber Chemistry and Technology*, Vol. 68, No. 4, 1995, pp. 660–670.

[2] Panda, B., Mychalowycz, E., and Tarzanin, F. J., "Application of Passive Dampers to Modern Helicopters," *Smart Materials and Structures*, Vol. 5, No. 5, 1996, pp. 509–516. doi:10.1088/0964-1726/5/5/001

[3] Felker, F., Lau, B., McLaughlin, S., and Johnson, W., "Nonlinear Behavior of an Elastomeric Lag Damper Undergoing Dual-Frequency Motion and its Effect on Rotor Dynamics," *Journal of the American Helicopter Society*, Vol. 32, No. 4, 1987, pp. 45–53.

[4] Zener, C. M., *Elasticity and Anelasticity of Metals*, Univ. of Chicago Press, Chicago, 1948.

[5] Gandhi, F., and Chopra, I., "A Time-Domain Non-Linear Viscoelastic Damper Model," *Smart Materials and Structures*, Vol. 5, No. 5, 1996, pp. 517–528. doi:10.1088/0964-1726/5/5/002

[6] Kunz, D. L., "Influence of Elastomeric Damper Modeling on the Dynamic Response of Helicopter Rotors," *AIAA Journal*, Vol. 35, No. 2, 1997, pp. 349–354.

[7] Tarzanin, F. J., and Panda, B., "Development and Application of Nonlinear Elastomeric and Hydraulic Lag Damper Models," 36th AIAA/ASME/ASCE/AHS/ASC Structures, Structural Dynamics, and Materials Conference, New Orleans, LA, AIAA, Paper 1995-1449, Apr. 1995.

[8] Krishnan, R., "Mechanisms-Based Analysis and Modeling of Elastomeric Lag Damper Behavior," M.S. Thesis, Department of Aerospace Engineering, Univ. of Maryland, College Park, MD, 2000.

[9] Snyder, R. A., "Mechanisms-Based Modeling of Filled Elastomeric Lag Damper Behavior," M.S. Thesis, Department of Aerospace Engineering, Univ. of Maryland, College Park, MD, 2001.

[10] Strganac, T. W., "An Experimental and Analytical Methodology to Characterize Nonlinear Elastomeric Lag Dampers," 38th AIAA/ASME/ASCE/AHS/ASC Stuctures, Structural Dynamics, and Material Conference, Orlando, FL, AIAA, Paper 1997-1153 , Apr. 1997.

[11] Lesieutre, G. A., and Bianchini, E., "Time-Domain Modeling of Linear Viscoelasticity Using Augmenting Thermodynamic Fields," *34th AIAA/ASME/ASCE/AHS/ASC Structures, Structural Dynamics, and Materials Conference*, Pt. 4, AIAA, Washington, DC, Apr. 1993, pp. 2101–2109.

[12] Lesieutre, G. A., and Mingori, D. L., "Finite Element Modeling of Frequency-Dependent Material Damping Using Augmenting Thermodynamic Fields," *Journal of Guidance, Control, and Dynamics*, Vol. 13, No. 6, 1990, pp. 1040–1050.

[13] Govindswamy, K., Lesieutre, G. A., Smith, E. C., and Beale, M. R., "Characterization and Modeling of Strain-Dependent Dynamics Behavior of Viscoelastic Elastomers in Simple Shear," 36th AIAA/ASME/ASCE/AHS/ASC Structures, Structural Dynamics, and Materials Conference, New Orleans, LA, AIAA, Paper 1995-1403Apr. 1995.

[14] Brackbill, C. R., Lesieutre, G. A., Smith, E. C., and Govindswamy, K., "Thermomechanical Modeling of Elastomeric Materials," *Smart Materials and Structures*, Vol. 5, No. 5, 1996, pp. 529–539. doi:10.1088/0964-1726/5/5/003

[15] Ramrakhyani, D. S., Lesieutre, G. A., and Smith, E. C., "Efficient Modeling of Elastomeric Materials Using Fractional Derivatives and

Plastic Yielding," 43rd AIAA/ASME/ASCE/AHS/ASC Structures, Structural Dynamics, and Materials Conference, Denver, CO, AIAA, Paper 2002-1436, Apr. 2002.

[16] Payne, A. R., and Whittaker, R. E., "Low Strain Dynamic Properties of Filled Rubbers," *Rubber Chemistry and Technology*, Vol. 44, No. 2, 1971, pp. 440–478.

[17] Timoshenko, S. P., *Strength of Materials*, Part 2, D. Van Nostrand, New York, 1933, pp. 679–680.

[18] Iwan, W. D., "Distributed-Element Model for Hysteresis and Its Steady-State Dynamic Response," *Journal of Applied Mechanics*, Vol. 33, No. 4, 1966, pp. 893–900.

[19] Iwan, W. D., "On a Class of Models for the Yielding Behavior of Continuous and Composite Systems," *Journal of Applied Mechanics*, Vol. 34, No. 3, 1967, pp. 612–617.

[20] Turner, D. M., "A Triboelastic Model for the Mechanical Behavior of Rubber," *Plastics and Rubber Processing and Applications*, Vol. 9, No. 4, 1988, pp. 197–201.

[21] Aklonis, J. J., and McKnight, W. J., *Introduction to Polymer Viscosity*, Wiley, New York, 1983.

[22] Constantinou, M., Mokha, A., and Reinhorn, A., "Teflon Bearings in Base Isolation, Part 2: Modeling," *Journal of Structural Engineering*, Vol. 116, No. 2, Feb. 1990, pp. 455–474.

[23] Berger, E. J., "Friction Modeling of Dynamic System Simulation," *Applied Mechanics Reviews*, Vol. 55, No. 6, Nov. 2002, pp. 535–577.
doi:10.1115/1.1501080

[24] Faires, J. D., and Burden, R., *Numerical Methods*, Brooks/Cole, Pacific Grove, CA, 1998.